Millimeter-Wave Multiplexed Wideband Wireless Link Using Rectangular-Coordinate Orthogonal Multiplexing (ROM) Antennas

Takashi Tomura, *Member, IEEE*, Jiro Hirokawa, *Fellow, IEEE*, Muhsin Ali, and Guillermo Carpintero, *Senior Member, IEEE*

***Abstract*—This paper is the first demonstration of multiplexed wideband data transmission in the millimeter-wave range using rectangular-coordinate orthogonal multiplexing (ROM) antennas. This spatial wireless multiplex communication method can be applied at several hundred GHz for further improvements in the data rate because much wider bandwidth is available and this multiplexing method does not require any signal processing. The multiplexing is achieved through the spatial eigenmodes of a novel antenna based on a rectangular coordinate system and magic-T which eliminates the need for computational signal processing efforts. The aperture distributions of these spatial eigenmodes are designed to have different polarities to avoid crosstalk and operate over a wide bandwidth range. We demonstrate their performance with four eigenmodes, achieving crosstalk between modes below −37.8 dB over a 14.6% relative bandwidth (57–66 GHz). We have introduced these antennas on a photonics-enabled real-time wireless data transmission, transmitting over two channels simultaneously, without any signal processing at the transmitter (multiplex) or the receiver (demultiplex). The two multiplexed channels show a total data rate up to 9.0 Gbps at most (5.875 Gbps and 3.125 Gbps for each channel) limited by the bandwidth of the low noise amplifiers at the receiver. The measured bit error rate (BER) is below the forward error correction (FEC) limit.**

***Index Terms*—Radio-over-fiber (RoF), real-time multiplex wireless communication, rectangular-coordinate orthogonal multiplexing (ROM), Spatial multiplex wireless communication, waveguide slot array antenna.**

I. Introduction

RECENT network forecasts show the explosive growth in wireless data traffic, urging to find new ways to increase data capacity [1]. The current available bandwidth allocated in the microwave range (3 to 30 GHz) is clearly insufficient and different ways to increase the capacity are being explored. It has become needed to open new portions of the spectrum where bandwidth is available, mainly in the millimeter-wave range (30 GHz to 300 GHz). Over the past years, regulatory bodies have been allocating spectrum bands for wireless communications in this range, starting with the historic 2003 ruling of the US Federal Communications Commission (FCC) to promote the use of this part of the spectrum, opening the E-band at 71–76 GHz, 81–86 GHz and 92–95 GHz (70/80/90 GHz). After the key milestone of Japan's NTT demonstrating a wireless link at 120 GHz carrier to provide live TV coverage at the 2008 Beijing Olympics [2], recent rulings have continued to open higher frequency bands above 100 GHz. In 2014, Japan allocated the 116–134 GHz band to accommodate such service, and more recently (March 15, 2019), the FCC freed a record 21.2 GHz of bandwidth for unlicensed use in the bands at 116–123 GHz, 174.8–182 GHz, 185–190 GHz, and 244-246 GHz [3]. The Terahertz frequency band [4][5], defined from 0.1 THz to 10 THz, is a prime candidate for ultra-high-data-rate short-distance LOS communication because of the large available bandwidths in that region, in contrast to the overcrowded sub-6 GHz frequency band [6]–[9]. For example, 260-Gbit/s wireless communication using 300-500 GHz has been demonstrated [8].

In addition to frequency bands with wider bandwidth, it is crucial to develop technologies to make efficient use of the available spectrum. Among the different techniques, spatial multiplexing greatly increases channel capacity and can be used in combination with other techniques, such as polarization multiplexing and high modulation schemes.

The polarization duplex is a method to increase channel capacity by using two orthogonal polarizations such as vertical and horizontal or left- and right-handed circular polarization. Another spatial multiplexing for a line of sight (LOS) communication is multiplexing by spatial eigenmodes. Orbital angular momentum (OAM) mode multiplexing uses spatial orthogonal eigenmodes which have phase variations in the circumference direction [10][11]. Each eigenmode creates an independent channel between Tx and Rx antennas and the channel capacity increases n times where n is the number of eigenmodes [12]–[15]. The great advantage of spatial eigenmode multiplexing is that it can realize more than the two degrees of multiplexing of the polarization duplex.

To date, the main drawback of OAM mode multiplexing is that the software-based multiplexing and demultiplexing are

Manuscript received March 30, 2021; revised May 28, 2021 and June 22, 2021; accepted June 24, 2021. Date of publication June 29, 2021; date of current version December 16, 2021. This work was supported in part by SEI Group CSR Foundation and the Murata Science Foundation. *(Corresponding author: Takashi Tomura.)*

Takashi Tomura and Jiro Hirokawa are with the Tokyo Institute of Technology, Tokyo 152-8552, Japan (e-mail: tomura@ee.e.titech.ac.jp; jiro@ee.e.titech.ac.jp).

Muhsin Ali and Guillermo Carpintero are with the Universidad Carlos III de Madrid, 28911 Madrid, Spain (e-mail: muali@ing.uc3m.es; guiller@ing.uc3m.es).

Color versions of one or more figures in this article are available at https://doi.org/10.1109/JLT.2021.3093445.

Digital Object Identifier 10.1109/JLT.2021.3093445

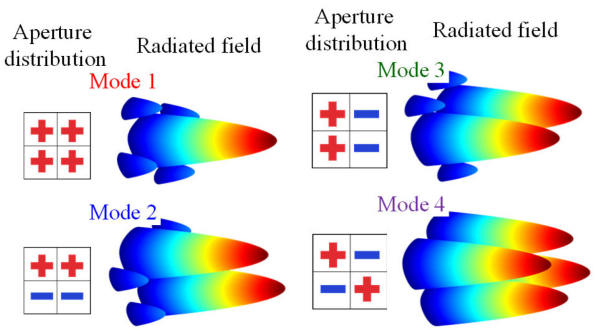

Fig. 1. Aperture distributions and radiated fields of four rectangular-coordinate spatial orthogonal eigenmodes.

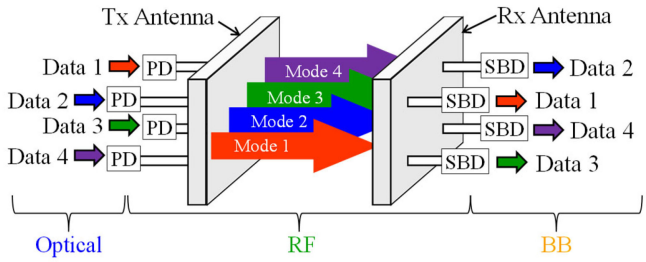

Fig. 2. Concept of ROM communications by four-mode rectangular orthogonal multiplex antennas.

challenging when the carrier frequency is high such as at several hundred GHz or terahertz [4][5]. Therefore, OAM multiplexing would benefit greatly from hardware multiplexing and demultiplexing, especially at the millimeter-wave range to enable multiplying the channel capacity by the number of eigenmodes. The OAM multiplexing uses spatial orthogonal eigenmodes which have uniform amplitudes and variated phase distributions in the circumference direction. Laguerre-Gaussian beam modes [16] are one of the eigenmodes used in OAM multiplexing, however, wideband generation of these phase distributions by hardware is difficult and bandwidth is limited [12]–[14]. This increases crosstalk among the multiple links and the signal to interference and noise ratio (SINR) deteriorates especially when wide bandwidths are used for communication. To overcome the hardware limitations, OAM-MIMO has been proposed and successfully demonstrated multiplex communication [17]–[19]. However, when the carrier frequency becomes very high and wide bandwidth is used, software processing becomes difficult. Therefore, hardware multiplexing and demultiplexing are desired especially for high-speed wireless links.

To overcome the drawbacks of OAM, rectangular-coordinate orthogonal multiplexing (ROM) has been proposed [20] and is suitable for hardware-based real-time wideband operation. Two spatial orthogonal eigenmode antennas are designed and used for multiplexing and are suitable for hardware-based real-time wideband operation. The eigenmodes are based on the rectangular coordinate system and have a different polarity of the field distribution. For example, the four lowest order eigenmodes have different polarities in four quadrants as shown in Fig. 1. These eigenmodes can be generated and separated by a magic-T [21][22] over a wide frequency range. The Hermite-Gaussian [16] beam is one among the eigenmodes which have different polarities in the subdivided region. We have previously demonstrated four-mode ROM antennas operating in the E-band [20] and V-band [23] for four multiplexing and four-mode dual-polarized ROM antennas in the V-band [24] for eight multiplexing. However, wireless data transmission has not been experimentally demonstrated so far. In the present work, we have for the first time used microwave photonic feed to excite the antennas.

In this paper, we present and experimentally demonstrate for the first time to the best of our knowledge, wideband hardware multiplexing and demultiplexing and establish a two-channel multiplexing wireless link using four-mode ROM antennas in the V-band as shown in Fig. 2. The V-band ROM antennas designed and characterized in [23] are used for ROM transmission. To make full use of the wider bandwidth of the antennas, the ROM antenna feeds are connected to a high-speed photodiode (HS-PD) with 100-GHz −3-dB bandwidth. The transmission signal is generated using microwave photonics techniques, using an optical heterodyne source which allows us to tune the carrier frequency over the entire HS-PD bandwidth, including the entire V-band range. Receiving antenna ports are connected to wideband Schottky barrier diodes (SBD) [25] to convert RF signals to baseband signals over the entire V-band range. Here, we demonstrate a two-channel ROM wireless link using the PD and the SBD with on-off-keying (OOK) modulation. Promising applications of fiber-based short-range wireless communication include front- and backhauling of base stations, wireless connections over difficult-to-access terrains such as a river, wireless connections in data centers.

II. Rectangular Orthogonal Mode Multiplexing

Multiplexing is realized by spatial orthogonal eigenmodes based on a rectangular coordinate system. Each eigenmode has a different combination of polarities in the subdivided region of the antenna aperture as suggested in Fig. 1. The radiated field from each of the aperture distributions shown in Fig. 1 has a different number of beams and the beam directions are different among the eigenmodes. For example, mode 1 has the same polarity in the subdivided regions and radiates a single beam in the boresight. Mode 2 has different polarities at the top and bottom in the antenna aperture and radiates two beams to the top and bottom directions. Hermite-Gaussian modes have similar aperture distributions and radiated fields. The Tx and Rx antennas have four ports and each port radiates and receives one of the four eigenmodes. Crosstalk between the modes can be suppressed over a wide bandwidth as will be discussed in the following section.

A. Antenna Structure and Performance Enabling ROM

The magic-T enables the generation and separation of the four orthogonal modes over a wide frequency band. A magic-T is a waveguide-based four-port microwave circuit as shown in Fig. 3(a). When a Σ port is excited, the input power is divided into two output ports with the same amplitude and in-phase. When a Δ port is excited, the input power is equally divided

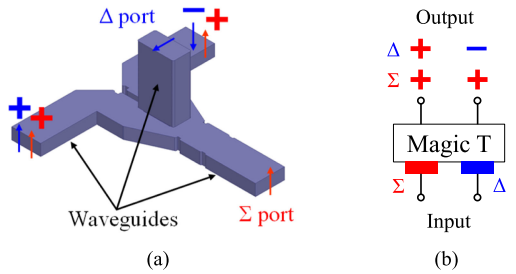

Fig. 3. (a) Structure of magic-T. (b) Output phase of the magic-T.

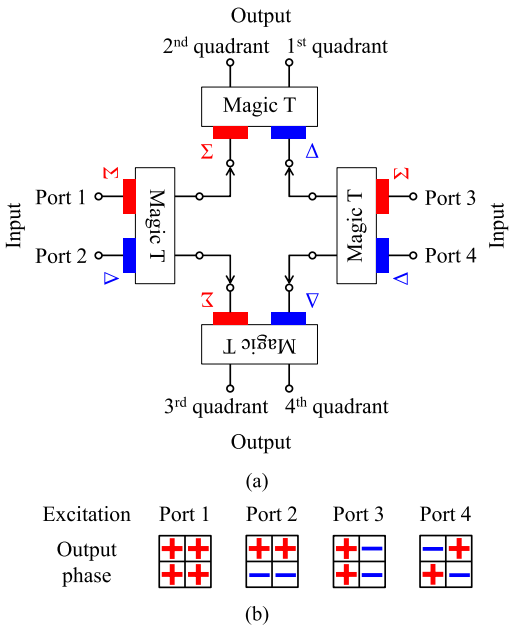

Fig. 4. Four ROM modes generation by magic-T. (a) Configuration of two-stage cascaded magic-T configuration. (b) Output phase distribution excited by each port.

into two output ports with the same amplitude and out-of-phase as shown in Fig. 3(b). The Σ port and the Δ port are isolated from each other. By connecting the four magic-T ports as shown in Fig. 4(a), four orthogonal modes are generated as shown in Fig. 4(b). When port 1 is excited, the four outputs have the same polarity in the four subdivided regions. When port 2 is excited, the two top outputs have plus polarity and the two other output ports have minus polarity.

An antenna that can generate and separate the four orthogonal modes consisting of four magic-T and waveguide slot arrays was designed. The antenna configuration shown in Fig. 5(a) is composed of a magic-T circuit, four corporate-feed circuits, and a radiation element shown in Fig. 5(b). The four magic-T circuits are connected as suggested in Fig. 4(a) to generate the four orthogonal modes and the magic-T circuit feeds the four corporate-feed circuits. The corporate-feed circuit feeds the radiation element with the optimum amplitude and phase to increase channel capacity [23]. The design targets of this antenna system are reflection < -9.54 dB (VSWR < 2), isolation $>$ 20 dB for 57–66 GHz and uniform transmission for four modes at 40-cm Tx-Rx distance at 61.5 GHz.

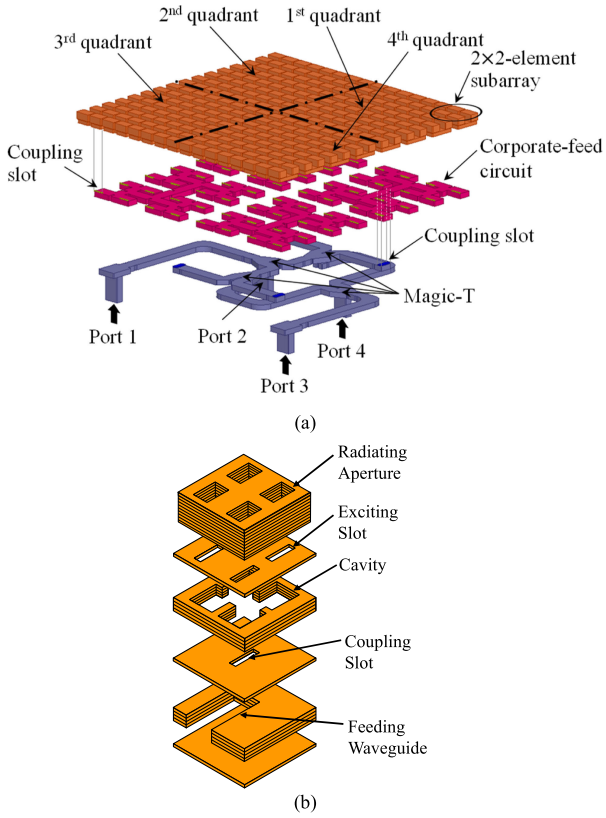

Fig. 5. (a) Four-mode ROM waveguide slot array antenna. (b) 2 × 2-element subarray.

The antenna was fabricated by diffusion bonding of etched thin copper plates. Simulated S-parameters are shown in Fig. 6 and reflection is below VSWR of 2 and isolation is 28 dB over 57–66 GHz. Measured S-parameters are available in [23] and the correspondence of simulated and measured reflection is good because the measured reflection is less than VSWR of 2 over 57–66 GHz. However, measured isolation was degraded compared with the simulated one. Especially measured S21 and S43 was 30 dB whereas simulated one is 50 dB.

B. Transmission Characteristics Between Two ROM Antennas

Wireless transmission between the two designed waveguide slot array antennas realizes high isolation for the four modes. The S-parameters between the two antennas with 40-cm separation were analyzed by an electromagnetic simulator, Ansys HFSS, based on a finite element method. 40 cm is selected because channel capacity starts to decrease when the transmission distance exceeds 40 cm as shown in Fig. 8 of [23]. When we increase the distance channel capacity decreases because radiated beam starts to diverge and transmission becomes lower and isolation degrades. When we decrease the transmission distance, channel capacity is almost unchanged because the radiated beam does not diverge yet. The results are shown in Fig. 7 and 0 dB corresponds to the direct connection of the waveguides without the antennas. The average transmissions from 57.0 GHz to 66.0 GHz are -3.9, -4.9, -5.4, and -6.4 dB for modes 1, 2, 3, and 4, respectively. The isolation is well suppressed over a wide bandwidth, with

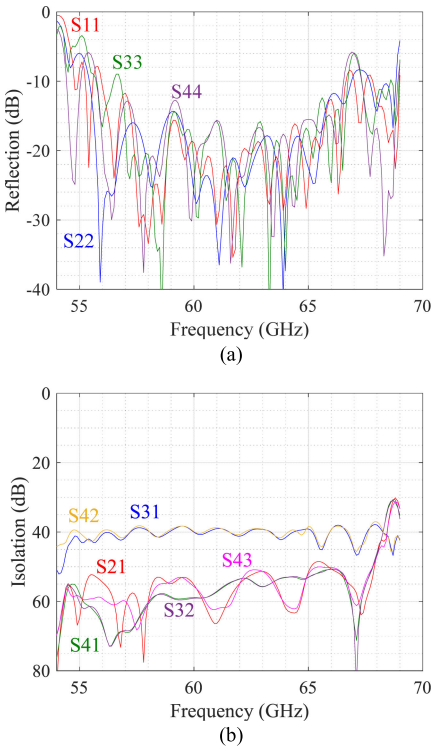

Fig. 6. Simulated S-parameters of the four-mode ROM waveguide slot array antenna. (a) Reflection. (b) Isolation.

the poorest value of −37.8 dB from 57.0 GHz to 66.0 GHz in mode 4.

Measured S parameters between the Tx and Rx antennas are also shown in Fig. 7. The isolation of the modes between the Tx and Rx antennas was degraded from −37.8 dB to −12.0 dB in the worst case. The measured S parameters show ripples because of multiple reflections between the Tx and Rx antennas. Hence, the isolation was calculated by averaging the measured S parameters over 57–66 GHz. This degradation results from fabrication tolerance of the ROM antenna and misalignment of the Tx and Rx antennas. The measured S parameters of the ROM antenna itself were degraded especially in isolation. This isolation degradation of the ROM antenna itself deteriorates the isolation between the Tx and Rx antennas. Misalignment of the antenna has a large impact on the isolation between the Tx and Rx antennas as discussed later in this section.

Isolation deteriorates by longer transmission distance and isolation of mode 4 deteriorates most quickly and that of mode 2 and 3 follows. Isolation is the ratio of desired main transmission signal $S_{i',i}$ to undesired cross-talk signals $S_{i',j}$ where $i' \neq j$. Main transmission changes by distance because of divergence of beam modes. As shown in Fig. 5(b) of [23], the transmission of mode 4 decreases most quickly among the four modes and mode 2 and 3 follows because the higher-order mode of beam mode diverges quickly compared with lower-order mode. Cross talk level does not change by distance and is determined by the performance of the ROM antenna itself especially magic-T. Our prototype of the antenna showed degraded isolation which

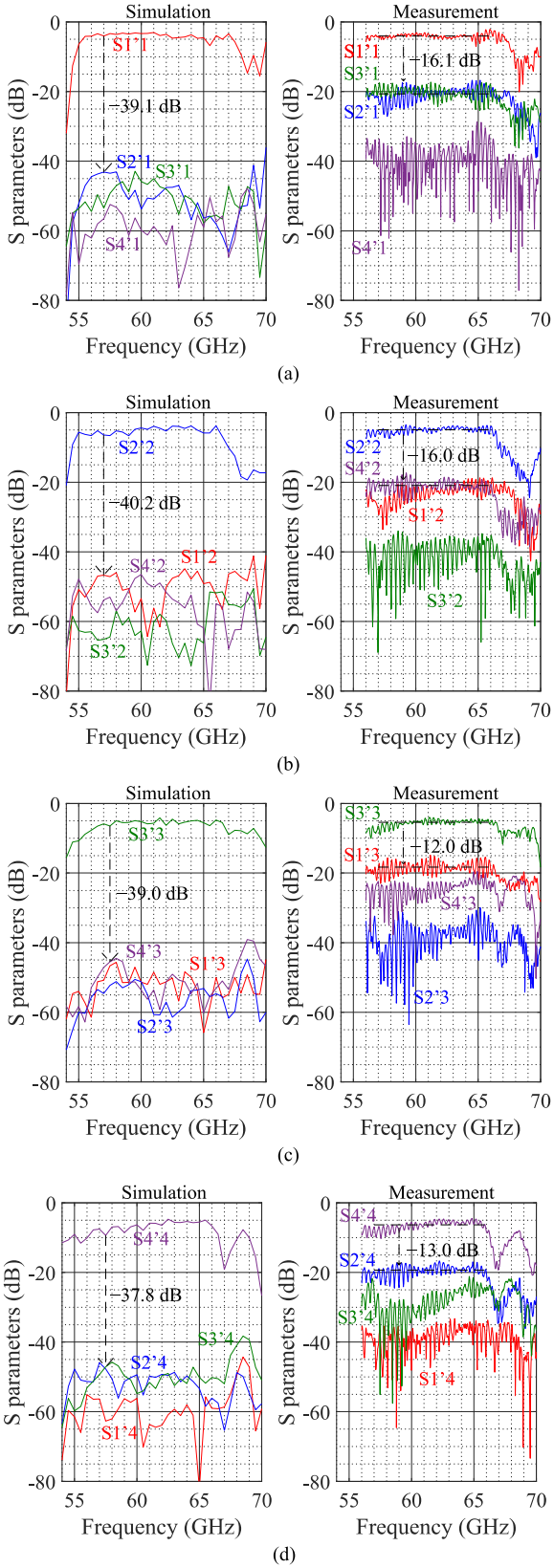

Fig. 7. Simulated and measured frequency characteristics of the S-parameters *Sij* (i = 1', 2', 3', 4', j = 1, 2, 3, 4) between the Tx (port 1, 2, 3, and 4) and Rx (port 1', 2', 3', and 4') antennas with 40-cm separation. (a) *Sij*, j = 1, (b) *Sij*, j = 2, (c) *Sij*, j = 3, (d) *Sij*, j = 4. The definition of the port number is depicted in Fig. 2.

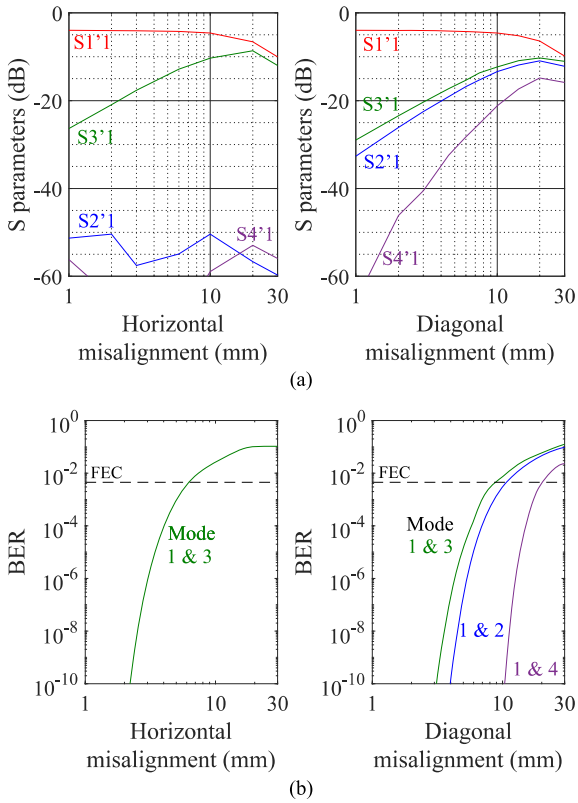

Fig. 8. Simulated horizontal and diagonal misalignment effect on (a) the S-parameters *Sij* (i = 1', 2', 3', 4', j = 1, 2, 3, 4) between the Tx (port 1, 2, 3, and 4) and Rx (port 1', 2', 3', and 4') antennas and (b) BER of a channel using mode 1.

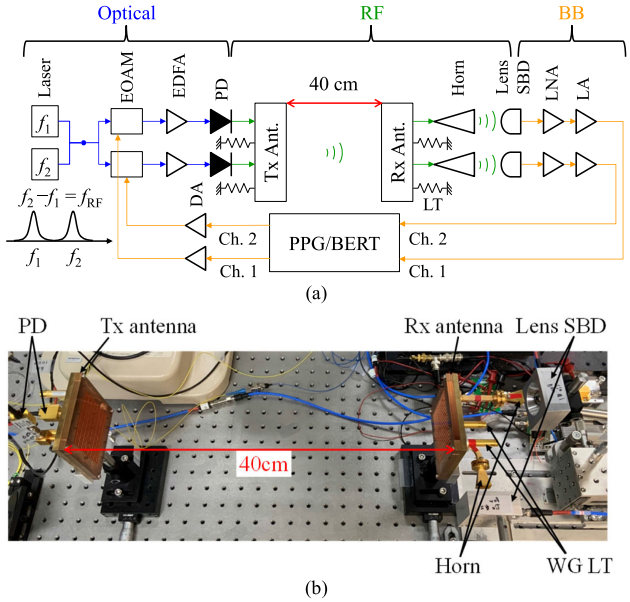

Fig. 9. Two-channel wireless data transmission test setup. (a) Schematic diagram of the transmission experiment setup. (b) Photo of the implemented transmission experiment setup. RF: radio frequency, BB: base band, EOAM: electro-optic amplitude modulator, EDFA: erbium doped fiber amplifier, PD: photodiode, Ant.: antenna, LT: load termination, SBD: Schottky barrier diodes, LNA: low noise amplifier, LA: limiting amplifier, Ch.: channel, PPG: pulse pattern generator, BERT: bit error rate tester, DA: driver amplifier, WG: waveguide.

results in the increment of cross-talk level. Therefore, when the distance increases, isolation of mode 4 deteriorate most by longer transmission distance and mode 2 and 3 follows.

Misalignment has a large impact on isolation resulting in degradation of BER. Simulated S parameters between Tx and Rx antennas with horizontal and diagonal misalignment are shown in Fig. 8(a). Horizontal misalignment breaks orthogonality between modes 1 and 3 and between modes 2 and 4 because of the aperture distributions of each mode shown in Fig. 4b. Isolation between modes 1 and 3 and between modes 2 and 4 is degraded by horizontal misalignment as shown in Fig. 8(a). Diagonal misalignment breaks orthogonality among all combinations of four modes and isolations of all mode combinations are degraded as shown in Fig. 8(a). BER of a channel using mode 1 is calculated from SNR which is assumed to be equal to the isolation between two modes. BER becomes larger than the FEC limit when the horizontal and diagonal misalignment is larger than 6.3 mm and 8.8 mm, respectively, as shown in Fig. 8(b).

III. Experimental Demonstration of the ROM

A. Measurement Setup

A two-channel wireless multiplexing communication measurement system was built and the multiplexing performance by the designed waveguide slot array antennas was evaluated. A schematic diagram of the transmission experiment setup is shown in Fig. 9(a). A pulse pattern generator (PPG) generates digital signals modulated by on-off-keying (OOK) and a bit error rate tester (BERT) measures the bit error rate (BER) of the received signals. Optical sub-carriers are generated by two 1550-nm continuous-wave lasers (f_1 and f_2) and modulated by an electro-optic amplitude modulator (EOAM). The optical signals are converted to RF signals by high-speed PIN photodiodes (PD). The wavelength of the lasers is determined so that $f_2 - f_1 = f_{RF} = 61.5$ GHz. The two PD are connected to the Tx antenna. The Rx antenna is placed to face the Tx antenna and the separation distance is maintained at 40 cm. The metal breadboard was covered by absorbers when the measurement was performed to reduce undesired reflection and scattering by the metal breadboard. The two Rx antenna ports are connected by WR-15 horn antennas to couple the received signal to the lens-mounted Schottky barrier diodes (SBD) [25]. The other ports of the Tx and Rx antennas are terminated by load terminations (LT). The PD has an interface of the 50-ohm 1.0-mm coaxial connector and both the ROM antenna and the horn have WR-15 waveguide interface. A 1.0-mm coaxial-to-waveguide adapter is used to connect the PD and the ROM antenna. The ROM antenna and the horn are connected using a standard WR-15 waveguide. The detected RF signals are converted to baseband (BB) signals by the SBD and then transmitted to the BERT through a low noise amplifier (LNA) and a limiting amplifier (LA). The transmitted signals are demodulated and BER is measured by the BERT in real-time.

B. Back-To-Back Measurement

Channels excluding the ROM antennas here are evaluated by directly connecting the PD and the horn antennas as shown in

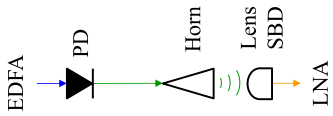

Fig. 10. Partially extracted schematic diagram of the direct-connected transmission experiment setup.

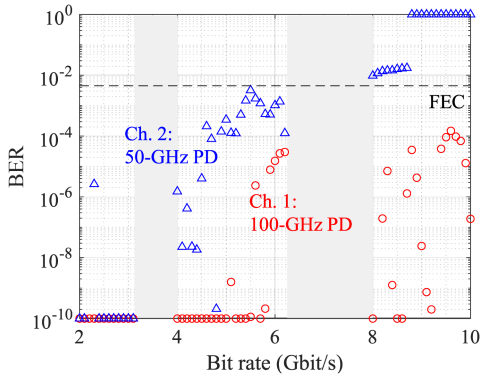

Fig. 11. Channel quality excluding the ROM antennas where photocurrents of the PD are fixed at 5.0 mA and 6.4 mA for channel 1 and 2, respectively.

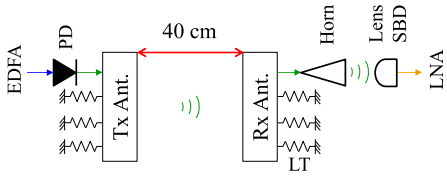

Fig. 12. Partially extracted schematic diagram of the direct-connected transmission experiment setup.

Fig. 10. Fig. 11 shows the BER characteristic dependence on bit rate for channel 1 using a 100-GHz PD. It realizes a BER of less than the FEC limit of 4.5×10^{-3} [26] up to 10 Gbit/s. Channel 2 using 50-GHz PD shows poorer BER characteristics than channel 1 because the carrier frequency is 61.5 GHz higher than the operating frequency of the 50-GHz PD. The bit rates in the range of 3.125−4.0 Gbit/s and 6.25−8.0 Gbit/s are not available in the PPG/BERT used in this experiment.

C. Single Channel

To further evaluate the transmission characteristics between the ROM antennas, a single-stream is here tested by the experiment setup shown in Fig. 12. The BER dependence on the bit rate is shown in Fig. 13. Compared to the directly connected case shown in Fig. 11, the BER of all modes is deteriorated because of imperfections in the transmission between the ROM antennas such as reduced transmitted power, limited bandwidth, group delays, and others. Here, it is important to mention that the reason why the BER does not increase monotonically is that multiple reflections occur between the Tx and Rx antennas, as well as in the interface between horn antenna and lens SBD and as communication quality deteriorates depending on the bandwidth.

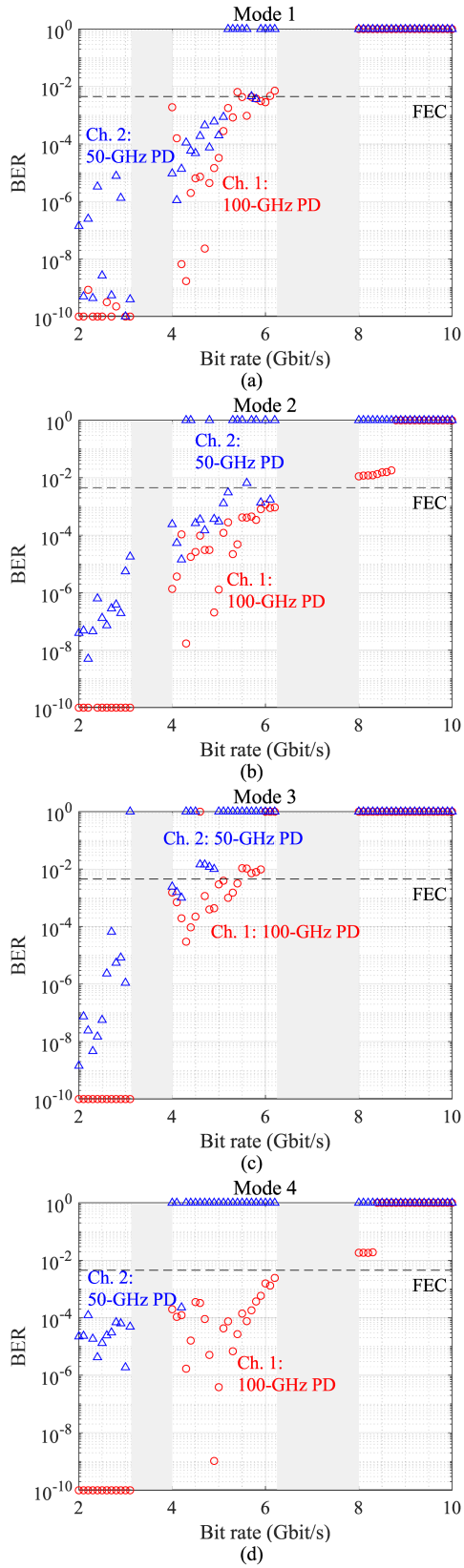

Fig. 13. Channel quality of the ROM antennas. (a) Mode 1, (b) Mode 2, (c) Mode 3, (d) Mode 4 where photocurrents of the PD are fixed at 5.0 mA and 6.4 mA for channel 1 and 2, respectively.

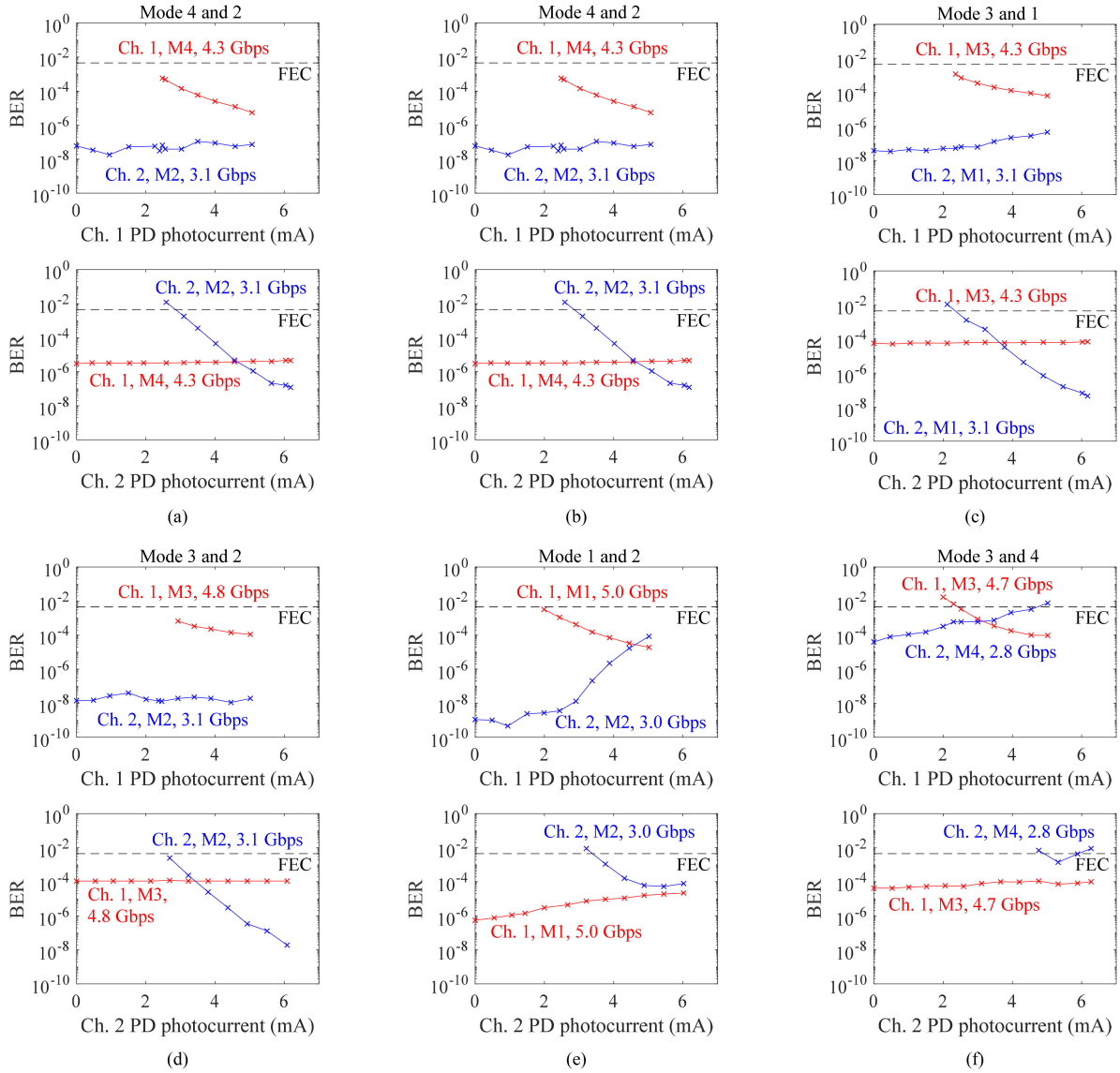

Fig. 14. Two-channel wireless transmission results. (a) Mode 4 and 2. (b) Mode 4 and 1. (c) Mode 3 and 1. (d) Mode 3 and 2. (e) Mode 1 and 2. (f) Mode 3 and 4. Ch.: channel, M: mode, FEC: forward error correction, PD: photodiode.

D. Two Channels

The two-channel wireless multiplexing communication with low interference between two modes was verified by the measurements. The measurement setup shown in Fig. 9 is used for the measurement. The BER characteristics are measured by varying the optical input power in one of the two PDs while maintaining a fixed output from the other. The measured results are shown in Fig. 14 for different two-mode combinations. The BER of channel 1 depends on the DC photocurrent of the PD used, and the BER of channel 2 remains low as shown in Fig. 14(a). Conversely, the BER of channel two depends on the photocurrent of channel 2, and as expected the BER of channel one remains low in the simulations. The same tendency is observed for the combinations of modes 1 and 4, 3 and 1, 3 and 2. However, with the mode combination of 1 and 2, the channel 1 photocurrent affects both channel 1 and 2 BER. This suggests that interference between modes 1 and 2 is not negligible. One of the reasons for the interference is that both modes 1 and 2 use the same first stage magic-T. A similar tendency is displayed in the 3 and 4 mode combination. The measured S parameter of the antenna itself [23] showed that S21 and S43 were degraded up to −30 dB where

TABLE I
MAXIMUM BIT RATE BELOW THE FEC LIMIT [26]

Ch. 1 (100-GHz PD)			Ch. 2 (50-GHz PD)			Total
Mode	Bit rate (Gbit/s)	BER	Mode	Bit rate (Gbit/s)	BER	Bit rate (Gbit/s)
1	5.000	3.0.E-04	2	3.000	4.7.E-04	8.000
3	5.200	7.0.E-04	1	3.125	6.6.E-11	8.325
4	5.600	8.1.E-04	1	3.100	2.3.E-08	8.700
3	5.600	6.0.E-04	2	3.100	7.6.E-08	8.700
4	5.875	2.2.E-04	2	3.125	7.9.E-08	9.000
3	5.100	1.8.E-04	4	3.100	1.5.E-04	8.200

Ch.: channel, PD: photodiode, BER: bit error rate.

TABLE II
COMPARISON OF SPATIAL MULTIPLEX WIRELESS COMMUNICATION

Ref.	Type	Carrier frequency (GHz)	Data rate (Gbit/s)	Data rate / single stream (Gbit/s)	Bandwidth, relative bandwidth	Modulation	Number of multiplex	Number of spatial mode	Data processing	Distance	Antenna area	Distance (λ_0) / antenna area (λ_0^2)
[12]	OAM	28	4.0	0.5	1 GHz 3.6%	16QAM	8 [a]	4	Offline	2.5 m $233\lambda_0$	0.070 m^2 $617\lambda_0^2$	0.38
[13]	OAM	60	32.0	8.0	2 GHz 3.3%	16QAM	4 [a]	2	Offline	2.5 m $500\lambda_0$	0.018 m^2 $708\lambda_0^2$	0.71
[14]	OAM	60	4.0	2.0	2 GHz 3.3%	QPSK	2	2	Offline	0.2 m $30\lambda_0$	0.018 m^2 $708\lambda_0^2$	0.04
[17]	OAM-MIMO	10	0.8	0.2	0.04 GHz 0.4%	32QAM	4	4	Offline	10.0 m $334\lambda_0$	0.280 m^2 $315\lambda_0^2$	1.06
[18]	OAM-MIMO	74.5	3.2	0.4	0.1 GHz 0.1%	16QAM	8	8	Offline	7.0 m $1739\lambda_0$	NA	NA
[19]	OAM-MIMO	40	100.0	7.1	1.5 GHz 3.8%	256QAM	14 [a]	7	Offline	117.0 m $15610\lambda_0$	1.100 m^2 $20133\lambda_0^2$	0.78
This work	ROM	61.5	9.0	4.5	9 GHz 14.6%	OOK	2	2	Real time	0.4 m $82\lambda_0$	0.004 m^2 $190\lambda_0^2$	0.43

λ_0 is a free space wavenumber at a carrier frequency
[a]Polaization duplex is used.

simulated S21 and S43 were −50 dB because of the fabrication tolerance of the first-stage magic-T. This degradation of the isolation between ports in Tx or Rx antenna causes interference between modes 1 and 2 and between modes 3 and 4.

The maximum total bit rate of channels 1 and 2 with BER less than a forward error correction (FEC) limit of 4.5×10^{-3} [26] is detailed in Table I. The maximum bit rate reaches 9.0 Gbit/s with modes 4 and 2. Because OOK modulation requires the double bandwidth of the bit rate, the 5.6 Gbit/s bit rate of channel 1 using mode 4 corresponds to 18.2% relative and an 11.2 GHz bandwidth. This suggests the wideband characteristics of this multiplexing method by ROM.

IV. DISCUSSION

The maximum obtainable bit rate for the ROM-based wireless setup alone is expected to be 18 Gbit/s and 36 Gbit/s for two- and four channels when QPSK and 9-GHz (57.0–66.0 GHz) bandwidth are used. The bit rate is estimated under the assumption that the SNR equals isolation and the measured S parameters are used to calculate the isolations. For the two-channel case, the worst isolation is 12.0-dB as shown in Fig. 7. For the four-channel case, total isolation is calculated by summation of transmission of the other three modes and the worst total isolation is 11.4 dB. When SNR is 11.4 dB, QPSK is available with BER less than 10^{-5}. Therefore, the maximum bit rate is expected to be 18 Gbit/s and 36 Gbit/s for two- and four-channel cases when QPSK and 9-GHz (57.0–66.0 GHz) bandwidth are used with a roll-off rate of 1 for the raised cosine filter.

Comparison of spatial multiplex wireless communications is shown in Table II. The highest bit rate of OAM type is 32 Gbit/s using 60-GHz band, 2 modes, polarization duplex, and 16QAM [13]. The one of OAM-MIMO type is 100 Gbit/s using a 40-GHz band using 7 modes, polarization duplex, and 256QAM [19]. However, their bandwidth is limited to less than 4% and the data were processed offline. The maximum bit rate of our proposing ROM is limited to 9.0 Gbit/s using 2 modes, single-polarization, and OOK. However, this work showed the largest bandwidth of 14.6% with real-time data processing. Therefore, ROM is suitable for wideband mode multiplex at the Terahertz frequency band.

Transmission distance is proportional to their antenna area when Tx and Rx antennas have the same area because the Rayleigh range of Hermite-Gaussian modes including higher-order mode is proportional to the cross-sectional area of beam waist [27]. Therefore, for example, when the transmission distance becomes twice, both the Tx and Rx antenna areas are required to be twice.

The longest transmission distance is 117.0 m ($15610\lambda_0$) using 1.1-m^2 ($20133\lambda^2{}_0$) antenna at the 40-GHz band. The efficiency of transmission distance over antenna area in wavelength is $0.78/\lambda_0$. The most efficient method is [17] and the efficiency is $1.06/\lambda_0$. The proposed ROM system has the efficiency of $0.43/\lambda_0$ and current efforts are directed towards improving the efficiency.

V. CONCLUSION

We have proposed a multiplexing method by spatial eigenmodes with different polarities and demonstrated two-channel wireless multiplexing communication. The spatial eigenmodes can be multiplexed and demultiplexed over wide bandwidths by magic-Tees. Crosstalk between different modes transmitted from Tx to Rx antennas is suppressed to less than −37.8 dB over a 14.6% relative bandwidth (57-66 GHz). Real-time two-channel wireless multiplexing is characterized by the measurements and low crosstalk has been confirmed. Changing the transmitted power of one channel does not affect the BER of the other channel. This suggests that crosstalk between the two modes

is sufficiently low. However, two of the mode combinations showed higher crosstalk levels. The maximum total data rate of 9.0 Gbps was confirmed using two-channel multiplexed wireless communication. Wideband hardware multiplexing and demultiplexing were shown by 5.6 Gbit/s bit rate of OOK modulation corresponding to 11.2 GHz and 18.2% relative bandwidth.

The proposed multiplex method can be applied to higher frequencies such as several hundred GHz because the spatial eigenmode can be multiplexed and demultiplexed only by the hardware with low crosstalk levels. The OAM multiplexing suffers from narrower bandwidths of crosstalk and requires signal processing to multiplex and demultiplex modes making it difficult to apply to the several hundred GHz bands. Different from OAM multiplexing, ROM multiplexing does not require software processing and is one of the most attractive candidates for achieving multiplexing at several hundred GHz bands. The required antennas can be fabricated by micromachining and have shown high-efficiency characteristics at several hundred GHz [28].

REFERENCES

[1] E. Ekudden, "Future network trends," Ericsson technology review, Sep. 2020 [Online]. Available: https://www.ericsson.com/4a58bc/assets/local/reports-papers/ericsson-technology-review/docs/2020/technology-trends-2020.pdf

[2] H. Takahashi, A. Hirata, N. Kukutsu, Y. Kado, T. Kosugi, and K. Murata, "Compact, low-power, 120-GHz-band wireless link for 10-Gbit/s data transmission," *NTT Tech. Rev.*, vol. 7, no. 3, pp. 1–6, 2009.

[3] [Online]. Available: https://docs.fcc.gov/public/attachments/FCC-19-19A1_Rcd.pdf

[4] T. Nagatsuma, G. Ducournau, and C. Renaud, "Advances in terahertz communications accelerated by photonics," *Nature Photon,* vol. 10, pp. 371–379, Jun. 2016.

[5] S. Koenig *et al.*, "Wireless sub-THz communication system with high data rate" *Nature Photon,* vol. 7, pp. 977–981, Dec. 2013.

[6] K. Takano *et al.*, "17.9 A 10 5 Gb/s 300 GHz CMOS transmitter," in *Proc. IEEE Int. Solid-State Circuits Conf.*, 2017, pp. 308–309.

[7] T. Nagatsuma *et al.*, "Real-time 100-Gbit/s QPSK transmission using photonics-based 300-GHz-band wireless link," in *Proc. IEEE Int. Topical Meeting Microw. Photon.*, 2016, pp. 27–30.

[8] X. Pang *et al.*, "260 Gbit/s photonic-wireless link in the THz band," in *Proc. IEEE Photon. Conf.*, 2016, pp. 1–2.

[9] T. Nagatsuma, T. Kurokawa, M. Sonoda, T. Ishibashi, M. Shimizu, and K. Kato, "600-GHz-band waveguide-output uni-traveling-carrier photodiodes and their applications to wireless communication," in *Proc. IEEE/MTT-S Int. Microw. Symp.*, 2018, pp. 1180–1183.

[10] L. Allen, M. W. Beijersbergen, R. J. C. Spreeuw, and J. P. Woerdman, "Orbital angular-momentum of light and the transformation of laguerre-gaussian laser modes" *Phys. Rev.*, vol. 45, pp. 8185–8189, Jun. 1992.

[11] G. Gibson *et al.*, "Free-space information transfer using light beams carrying orbital angular momentum" *Opt. Exp.*, vol. 12, pp. 5448–5456, Nov. 2004.

[12] Y. Yan *et al.*, "High-capacity millimetre-wave communications with orbital angular momentum multiplexing," *Nature Commun.*, vol. 5, no. 1, Dec. 2014, Art. no. 4876.

[13] Y. Yan *et al.*, "32-Gbit/s 60-GHz millimeter-wave wireless communication using orbital angular momentum and polarization multiplexing," in *Proc. IEEE Int. Conf. Commun*. 2016, pp. 1–6.

[14] Z. Zhao *et al.*, "A dual-channel 60 GHz communications link using patch antenna arrays to generate data-carrying orbital-angular-momentum beams," in *Proc. IEEE Int. Conf. Commun.*, 2016, pp. 1–6.

[15] Y. Zhang and J. Li, "Analyses and full-duplex applications of circularly polarized OAM arrays using sequentially rotated configuration," *IEEE Trans. Antennas Propag.*, vol. 66, no. 12, pp. 7010–7020, Dec. 2018, doi: 10.1109/TAP.2018.2872169.

[16] A. E. Siegman, *Lasers*, Mill Valley, CA, USA: Univ. Sci. Books, 1986.

[17] W. Zhang *et al.*, "Mode division multiplexing communication using microwave orbital angular momentum: An experimental study," *IEEE Trans. Wireless Commun.*, vol. 16, no. 2, pp. 1308–1318, Feb. 2017.

[18] T. Nguyen, M. Hirabe, H. Miyamoto, R. Zenkyu, M. Uchida, and E. Sasaki, "An experimental study of high-capacity link using orbital angular momentum mode multiplexing in E-band," in *Proc. Int. Symp. Antennas Propag.*, 2018, pp. 1–2.

[19] H. Sasaki, Y. Yagi, T. Yamada, T. Semoto, and D. Lee, "An experimental demonstration of over 100 Gbit/s OAM multiplexing transmission at a distance of 100 m on 40 GHz band," in *Proc. IEEE Int. Conf. Commun. Workshops*, 2020, pp. 1–6.

[20] K. Tekkouk, J. Hirokawa, and M. Ando, "Multiplexing antenna system in the non-far region exploiting two-dimensional beam mode orthogonality in the rectangular coordinate system," *IEEE Trans. Antennas Propag.*, vol. 66, no. 3, pp. 1507–1515, Mar. 2018.

[21] N. Marcuvitz, *WaveguideHandbook*, New York, NY, USA: McGraw-Hill, 1951.

[22] D. M. Pozar, *Microwave Engineering*, 4th ed., New York, NY, USA: John Wiley & Sons, 2011.

[23] R. Ohashi, T. Tomura, and J. Hirokawa, "Transmission enhancement in rectangular-coordinate orthogonal multiplexing by excitation optimization of slot arrays for a given distance in the non-far region communication," *IEICE Trans. Commun.*, vol. E103-B, no. 2, pp. 130–138, Feb. 2020, [Online]. Available: https://t2r2.star.titech.ac.jp/rrws/file/CTT100816214/ATD100000413/

[24] K. Wada, T. Tomura, and J. Hirokawa, "Dual-polarized two-dimensional beam mode orthogonal multiplexing antenna system for the non-far region," *IEEE Trans. Antennas Propag.*, vol. 68, no. 9, pp. 6614–6623, Sep. 2020.

[25] M. Ali *et al.*, "Quasi-optical schottky barrier diode detector for mmWave/sub-THz wireless communication," in *Proc. Int. Conf. Telecommun.*, 2018, pp. 1–4.

[26] F. Chang, K. Onohara, and T. Mizuochi, "Forward error correction for 100 g transport networks" *IEEE Commun. Mag.*, vol. 48, no. 3, pp. S48–S55, Mar. 2010.

[27] J. T. Luxon, D. E. Parker, and J. Karkheck, "Waist location and rayleigh range for higher-order mode laser beams," *Appl. Opt.*, vol. 23, no. 13, pp. 2088–2090, 1984.

[28] A. Gomez-Torrent *et al.*, "A 38 dB gain, low-loss, flat array antenna for 320–400 GHz enabled by silicon-on-insulator micromachining," *IEEE Trans. Antennas Propag.*, vol. 68, no. 6, pp. 4450–4458, Jun. 2020.

Takashi Tomura (Member, IEEE) received the B.S., M.S., and D.E. degrees in electrical and electronic engineering from the Tokyo Institute of Technology, Tokyo, Japan, in 2008, 2011, and 2014, respectively. From 2014 to 2017, he was with Mitsubishi Electric Corporation, Tokyo, Japan, and was engaged in research and development of aperture antennas for satellite communications and radar systems. From 2017 to 2019, he was a Specially Appointed Assistant Professor with the Tokyo Institute of Technology. He is currently an Assistant Professor there. His research interests include electromagnetic analysis, aperture antennas, and planar waveguide slot array antennas. In 2013, he was a Research Fellow of the Japan Society for the Promotion of Science. Dr. Tomura was the recipient of the Best Student Award from Ericsson Japan in 2012 and the IEEE AP-S Tokyo Chapter Young Engineer Award in 2015 and Young Researcher Award from IEICE technical committee on antennas and propagation in 2018. He is a Member of the IEICE.

Jiro Hirokawa (Fellow, IEEE) received the B.S., M.S., and D.E. degrees in electrical and electronic engineering from the Tokyo Institute of Technology (Tokyo Tech), Tokyo, Japan, in 1988, 1990, and 1994, respectively. He was a Research Associate from 1990 to 1996 and an Associate Professor from 1996 to 2015 with Tokyo Tech. He is currently a Professor there.

From 1994 to 1995, he was a Postdoctoral Fellow with Antenna Group, Chalmers University of Technology, Gothenburg, Sweden. His research interests include slotted waveguide array antennas and millimeter-wave antennas. He was the recipient of the IEEE AP-S Tokyo Chapter Young Engineer Award in 1991, Young Engineer Award from IEICE in 1996, Tokyo Tech Award for Challenging Research in 2003, Young Scientists' Prize from the Minister of Education, Culture, Sports, Science and Technology in Japan in 2005, Best Paper Award in 2007 and Best Letter Award in 2009 from IEICE Communications Society, and IEICE Best Paper Award in 2016 and 2018. He is a Fellow of IEICE.

Muhsin Ali received the B.S. degree in telecom engineering from NUCES, Pakistan, in 2011, the M.S. degree in electrical engineering from NUST, Pakistan, in 2013, and the Doctorate degree in electrical, electronics and automation engineering from Universidad Carlos III de Madrid (UC3M), Getafe, Spain, in 2020. He was an RF Engineer with Huawei, Saudi Arabia. His research interests include the design, fabrication and integration aspects of mm-Wave and THz photonic emitters and electronic detectors for high-speed wireless links with beam-steering capabilities aimed at beyond 5G systems. During the Ph.D., he was a Visiting Researcher with Fraunhofer Heinrich Hertz Institute, Berlin, Germany, in 2019. He is currently a Research Associate with UC3M, where his research focuses on designing dielectric waveguide-based THz interconnects and phased array antennas for the applications in instrumentation, sensing and wireless systems. Dr. Ali was the recipient of the Young Scientist Award from URSI-GASS in 2020.

Guillermo Carpintero (Senior Member, IEEE) received the Telecommunication Engineering degree from Universidad Politécnica de Madrid, Madrid, Spain, in 1994 and the Ph.D. degree from Universidad Carlos III de Madrid, Getafe, Spain, in 1999. Since 2017, he has been a Full Professor with Universidad Carlos III de Madrid, where he has started the research line on integrated microwave photonics. He has authored or coauthored around 200 articles and conference contributions on photonic integrated microwave, millimeter- and Terahertz-wave devices and systems, having delivered two keynote and 24 invited talks in various international conferences. His current interests include photonic hybrid integration and photonic-enabled millimeter-wave antenna arrays. He is a Member of the Board of Stakeholders of the Photonics21 European Technology Platform, Co-Ordinator of the RF Photonics and Wireless Application Interest Group (AIG) of the International Integrated Photonic Systems Roadmap (IPSR-I), and a MC Member of the EU COST 16220: European Network for High Performance Integrated Microwave Photonics. He has served on the programme committees for many international conferences.